# Numerical analysis of the stressed state of composite plates with a core layer made of tetrachiral honeycombs under static bending

Alexey V. Mazaev, Marina V. Shitikova

Composites Part C: Open Access 6 (2021) 100217

Contents lists available at ScienceDirect

Composites Part C: Open Access

journal homepage: www.sciencedirect.com/journal/composites-part-c-open-access

# Numerical analysis of the stressed state of composite plates with a core layer made of tetrachiral honeycombs under static bending

Alexey V. Mazaev [b], Marina V. Shitikova [a,b,*]

[a] National Research Moscow State University of Civil Engineering, 26, Yaroslavskoye Shosse, Moscow, Russia
[b] Voronezh State Technical University, Research Center on Dynamics of Solids and Structures, 84, st. 20-letija Oktyabrya, Voronezh, 394006, Russia

ARTICLE INFO

*Keywords:*
Composite plates
Tetrachiral honeycombs
Geometric discretization
Relative density
Finite element method
Stress distribution

ABSTRACT

The present work considers three-layer composite plates with solid face layers and a honeycomb core layer of the tetrachiral type. Under static bending conditions, the effects of discretization (the number of unit cells), relative density and thickness of tetrachiral honeycombs on the stressed state of composite plates are studied. Two sets of numerical experiments have been conducted: within the first one, the thicknesses of layers of composite plates have been remained constant with the variation in the volume of solid body of honeycombs, and in the second case, the volume of solid body of honeycombs is constant under the variation in the thickness of the honeycomb structures. Numerical modeling has been carried out within the framework of the theory of elasticity using the Comsol Multiphysics finite element analysis software, as well as with help of the finite element algorithms for solving the plane problem of the theory of elasticity. Based on the results of the analysis, diagrams of the honeycomb core relative density and thickness dependence of the maximal stresses in the layers of composite plates are presented, respectively, for the first and second formulation of numerical experiments. It has been shown that the discretization of tetrachiral honeycombs provides a significant effect on the strength of the honeycombs. Variation in the honeycombs thickness via changing the relative density under the constant volume of honeycombs solid body also has a significant effect on the strength of the composites.

## 1. Introduction

Currently, interest in materials with negative Poisson's ratio (auxetics), which exhibit the inverse deformation mechanism: expand/contract under tension/compression [1], does not subside. There is a large number of theoretical and experimental works that discuss the auxetic behavior of various kinds of materials [2–6]. However, the theoretical admissibility of the existence of materials with negative Poisson's ratio (NPR) was first shown by Love more than a century ago [7], and later in Landau and Lifshits [8]. As compared with classical materials, auxetics demonstrate advantages in mechanical behavior [9], for example, they show increased energy absorption, increased resistance to indentation and to the process of initiation and opening of cracks. These advantages have always been of interest to manufacturers of materials, often such properties are combined in composite structures. One of the modern trends is the development of sandwich composites with honeycomb core layers of non-standard geometry [10, 11], where auxetic honeycombs as core layers can remarkably complement classical materials.

Lorato et al. [12] described the mechanical behavior of tri-chiral, tetrachiral, and hexachiral honeycomb structures in the out-of-plane direction. Analytical expressions were proposed to determine the transverse Young's modulus and the Voigt and Reuss bounds for the transverse shear stiffness. Using finite element analysis, the analytical results were verified, and the effect of honeycombs thickness on transverse shear stiffness was determined. The theoretical models have been verified through experiments on specimens obtained by additive technologies.

Alderson et al. [13] determined the values of Young's modulus and Poisson's ratio for a number of chiral honeycomb structures. The authors applied numerical analysis using the finite element modeling and ambient experiments on nylon specimens. It has been shown that a family of chiral honeycombs could exhibit auxetic behavior.

Some results were presented at the 1st International Conference on Computations for Science and Engineering (ICCSE1), an online event, July 19–20, 2021, as well as at the International Conference of Young Scientists and Students «Topical Problems of Mechanical Engineering» (ToPME-2020), an online event, December 2–4, 2020.

* Corresponding author.
*E-mail address:* mvs@vgasu.vrn.ru (M.V. Shitikova).

https://doi.org/10.1016/j.jcomc.2021.100217
Received 19 October 2021; Received in revised form 27 November 2021; Accepted 4 December 2021
Available online 5 December 2021

Chen et al. [14, 15] described the mechanical behavior of a rectangular (tetrachiral) lattice using the plane orthotropic micropolar theory. Under the assumption of the stiffness of the lattice circles, the authors derived analytical expressions for 13 effective constants of a micropolar material. They also proposed a numerical homogenization procedure that takes into account the deformability of the lattice circles, and showed that deformation of the circle affects the chiral, mechanical, and auxetic behavior of the lattice. Young's modulus and Poisson's ratio of tetrachiral structures depend on the orientation of the load, as a result of which tetrachiral honeycombs exhibit auxeticity only in a narrow range of directions, in contrast to trichiral structures.

Bacigalupo and Gambarotta [16] considered the non-local homogenization of the hexachiral and tetrachiral honeycomb structures using two approaches. In the first case, the structure was represented as a beam-lattice with subsequent homogenization in the form of a micropolar continuum. The second approach proposed by the authors considered periodic cells from deformable portions by means of the second gradient homogenization. Bacigalupo and Gambarotta derived analytical expressions for the effective honeycomb structures constants using micropolar homogenization. They also showed the dependence of Young's modulus and Poisson's ratio of tetrachiral structures on the orientation of uniaxial stress.

According to the results in [14–16], tetrachiral honeycomb structures under uniaxial deformation along the main directions in the plane exhibit zero Poisson's ratio, which is inconsistent with the experimental results [13].

Mousanezhad et al. [17] carried out theoretical and numerical studies of the mechanical behavior of chiral and hierarchical honeycomb structures, the geometric features of which occur in nature. The energy-based approach was used to study the elastic constants. As a result, analytical expressions were derived for the effective Young's modulus, shear modulus and Poisson's ratio of chiral, antichiral and hierarchical honeycomb structures based on a square and a hexagon. Analytical results have been numerically verified using the finite element method. The authors showed that hierarchy and chirality have a significant influence on the mechanical properties of structures.

Zhong et al. [18] derived analytical expressions for the effective Young's modulus, shear modulus, and Poisson's ratio of tetrachiral honeycombs. The authors used the method of elliptic integrals based on Timoshenko's theory for bending beams with a large deflection. The theoretical results were verified using numerical calculations. When modeling the nonlinear mechanical behavior of tetrachiral honeycombs, it has been found that Poisson's ratio has positive values in tension and negative values in compression. The authors explained this behavior by the influence of the relationship between shear and normal deformation under uniaxial loading. In addition, in nonlinear modeling, Poisson's ratio has exhibited a dependence on the magnitude of deformation, and in linear modeling it turned out to be zero, what agrees with the results in [17].

Qi et al. [19] investigated the deformation of tetrachiral auxetic honeycombs under quasi-static and dynamic uniaxial compression using numerical and theoretical methods, as well as ambient experiments. Under quasi-static longitudinal compression, the tetrachiral honeycombs exhibited uneven transverse compression in the «Z» mode, as a result of which a sloping band of deformed unit cells appeared in the middle of the experimental specimen, dividing the specimen in two parts. Along the edges of the sloping band, bulges with a lower relative density were formed. Under dynamic longitudinal compression, the tetrachiral honeycombs exhibited a sequential zigzag compaction of the specimen in the «I» mode with uniform transverse contract. The authors explained the absence of bulges during dynamic deformation by the lag of the stress wave in the honeycomb structure in comparison with the shock wave. With an increase in the coefficient $\alpha_h$ (the ratio of the radius of the cylinders and the length of tangentially attached ribs), the strength under quasi-static and dynamic compression monotonically increased, and the bulge effect also decreased. However, for specimens with the same relative density, the coefficient $\alpha_h$ almost did not affect the strength under dynamic compression. Qi et al. [19] proposed analytical expressions for determining plateau stress in two sets of experiments. In addition, the authors determined the Poisson's ratio in the plane for tetrachiral honeycombs under quasi-static and dynamic compression using the finite element method. NPR was determined by the displacement of two representative nodes without taking the resulting bulges into account. Simulation under conditions of quasi-static compression at small deformations showed the dependence of Poisson's ratio on the magnitude of deformation. Under dynamic loading, an increase in impact velocity increased the NPR value. With a decrease in the coefficient $\alpha_h$, the NPR of tetrachiral honeycombs monotonously decreased. The analytical expression for determining the minimum value of the effective Poisson's ratio at the provisional densification strain under conditions of quasi-static compression was proposed.

Alomarah et al. [20] investigated the known honeycomb structures under quasi-static uniaxial compression: re-entrant, tetrachiral, and anti-tetrachiral, as well as the deformation process, energy absorption efficiency and NPR values. A new re-entrant chiral structure was also studied via numerical modeling by the finite element method and ambient experiments. Experimental specimens were made from polyamide using additive technologies. Under quasi-static compression, the tetrachiral honeycombs exhibited a sequential zigzag compaction without a pronounced deformation mode «Z» [19], but rather in a deformation mode «I» with a minimal bulge effect. Taking into account the small value of the coefficient $\alpha_h$ for the specimens in [20], the results obtained agree poorly with the results of [19]. During numerical and ambient experiments, the NPR of tetrachiral honeycombs did not exhibit a pronounced dependence on the magnitude of the compression deformation in comparison with the results reported in [18, 19]. When calculating Poisson's ratio, instead of two representative nodes [19], the authors used ten representative nodes from the central part of the honeycombs to determine the average displacements in the longitudinal and transverse directions. As a result of numerical and ambient experiments, tetrachiral honeycombs have exhibited the highest value of Young's modulus.

Lu et al. [21] have numerically and theoretically investigated the auxetic behavior of tetrachiral honeycomb structures. The presence of a relationship between shear and longitudinal deformation in tetrachiral honeycombs under uniaxial loading leads to ambiguity in the determination of Poisson's ratio. From [17] it is known that the traditional method of calculating Poisson's ratio using the compliance matrix does not show negative values. However, in ambient experiments, tetrachiral honeycombs exhibit auxetic behavior [13, 20]. An alternative description of auxeticity based on a representative volume element with periodic boundary conditions was applied in [21]. The circles of the structure were considered as rigid, and the attached ribs were deformed according to the theory of the Euler beam. As a result, the authors proposed a numerical approach to determine the effective Poisson's ratio using a stiffness or compliance matrix. An analytical expression considering the geometric parameters of tetrachiral honeycombs was proposed for calculating the effective Poisson's ratio.

The works considered above demonstrate that the analytical description and numerical determination of the Poisson's ratio of tetrachiral honeycombs do not always show their auxeticity, however, ambient experiments unambiguously determine the NPR of tetrachiral honeycombs. The study of the mechanical behavior of chiral structures using the finite element method is a convenient and proven approach, but this method is also ambiguous in determining the NPR of tetrachiral honeycombs. At the same time, auxeticity could have an additional effect on the stiffness and strength of honeycomb structures. Based on the analytical expressions in [19] and [21] for determining the NPR of tetrachiral honeycombs, it could be concluded that with an increase in the relative density of honeycombs Poisson's ratio goes from negative values to positive ones. This dependence will be graphically demonstrated in

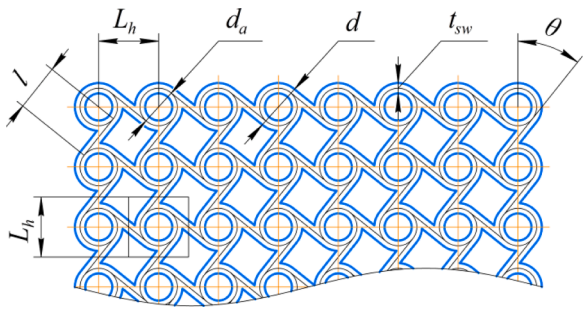


**Fig. 1.** Parameters of the honeycomb structure of tetrachiral type.

Section 3.

Scarpa and Tomlinson [22] have shown theoretically that re-entrant honeycomb core layers increase the stiffness of composite plates under flexural conditions. In [23] it has been demonstrated via numerical simulations and experiments that the re-entrant honeycomb exhibits a higher specific stiffness in bending compared to hexagonal honeycombs. Li and Wang [24] investigated the mechanical behavior of sandwich composites with honeycomb core layers of various types. As a result, it has been revealed that re-entering honeycombs have high energy absorption and exhibit efficient stress distribution.

Xiao et al. [25] numerically and experimentally studied the behavior of a sandwich beam with re-entrant honeycombs under conditions of a local shock pulse and rigid fixation. The experimental specimens were made of aluminum alloy using additive technologies. It is shown that the small wall thickness of the re-entrant honeycombs leads to the auxetic behavior of the structure and local compaction during a shock pulse, while the large wall thickness of the re-entrant honeycombs results in a global deformation of the structure with classical behavior.

Essassi et al. [26] investigated the behavior of a sandwich beam with re-entrant honeycombs under three-point bending conditions. Experimental specimens were made from biological material using additive printing. The effect of the relative density of honeycomb core layers on the stiffness of composites under bending and shear loads has been studied.

Sandwich composites with auxetic honeycombs were investigated numerically and experimentally in [27, 28] under three-point bending conditions. Experimental specimens were made from wood-based materials, in so doing the stiffness, strength, and the ability of the studied composites to absorb energy have been determined. The results show the superiority of auxetic honeycomb structures over classical honeycombs. The cases when the plane of honeycomb structures with auxetic behavior is located collaterally and perpendicular to the plane of composite panels have been considered, respectively, in [22,23, 26-28] and [24, 25].

In the present work, three-layered composite plates with solid face layers and a honeycomb core layer of tetrachiral geometry are considered. This structure consists of ordered cylinders arranged in a square grid pattern, which are connected to each other by tangentially attached ribs, wherein each of the cylinders involves four attached ribs [12–21]. Similar composites were investigated in [29] under conditions of bending with rigidly clamped ends, where the effect of discretization and the relative density of honeycombs on the strength of composite plates was also studied. When modeling composites, a non-uniform step for increasing the volume of a honeycombs solid body was adopted, and the loading condition resulted in redundant bending of the composite plates along the width. These shortcomings of [29] were eliminated in [30] by means of a refined formulation for two sets of numerical experiments, as well as for the case of three-point bending of plates. In contrast to [29] and [30] in the present work, the effects of discretization and honeycombs relative density on the stressed state of composite plates under conditions of bending with rigidly clamped ends have been studied in detail. Photopolymer resin is used as the material for composites, what simplifies the verification of numerical experiments in the framework of ambient experiments. In addition, the second set of numerical experiments has been carried out with the aim of revealing the influence of the variation in the thickness of the honeycomb structures on the strength of composite plates at a constant volume of honeycombs solid body.

## 2. Problem formulation

Let us consider tetrachiral honeycombs, the plane of auxetic behavior of which is parallel to the plane of composite plates. Honeycombs have been designed at four magnitudes of the size of unit cells $L_h = 1.6d_a$, where $d_a \in$ 1, 1.3, 1.6, and 1.9. For the given honeycombs, the following geometric parameters have been used (Fig. 1): at $r_a/l = const$ $(r_a = d_a/2)$, $\theta = const$, while $\alpha = l/r \approx const$ $(r = d/2)$ and $\beta = t_{sw}/r \approx const$ at $\rho_{rel} = const$.

Thus, tetrachiral honeycombs have been designed with different discretization (the number of unit cells), which depends on the parameter $L_h$, as well as with an equal range of change in the relative density $\rho_{rel}$ (%), which is defined as the ratio of the volume of solid body of the honeycombs to the volume of the interlayer bounded by the outer faces. The volume of a solid body of the honeycomb structures could be varied by changing the thickness of their walls $t_{sw}$. At each of the four values of $L_h$, the tetrachiral honeycombs uniformly fill the interlayer of the composites.

For further numerical analysis, let us consider plates with the length $a$, width $h$ and thickness $t$ (Fig. 2) rigidly supported within the areas $0 \le x \le x_1$ and $x_2 \le x \le a$ for the case when they are subjected to the

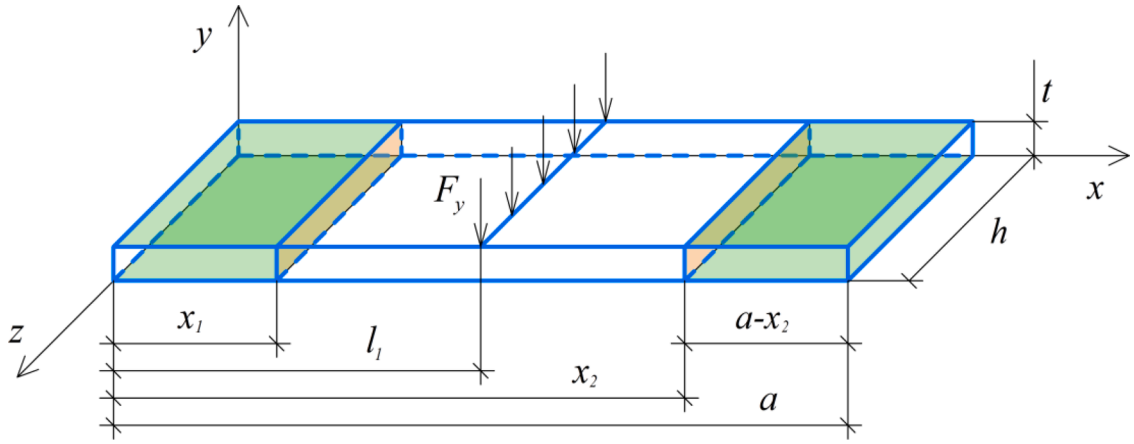


**Fig. 2.** Loading condition and boundary conditions for composite and solid plates.

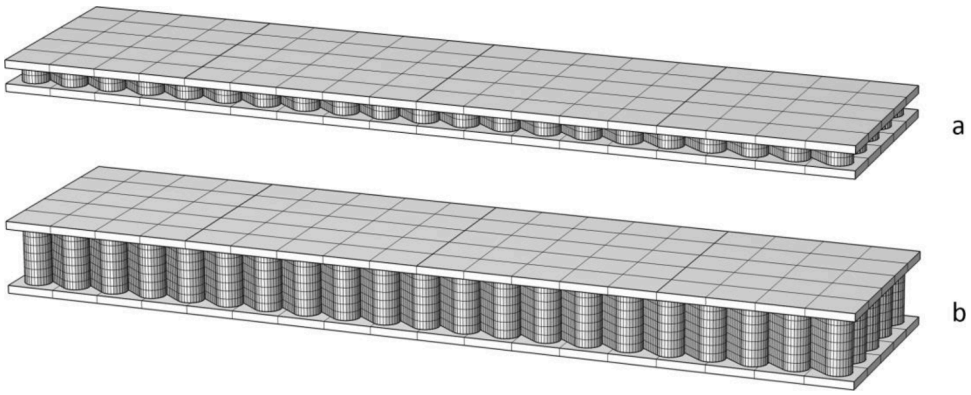


**Fig. 3.** The finite element mesh of a thin (a) and relatively thick (b) composite plate.

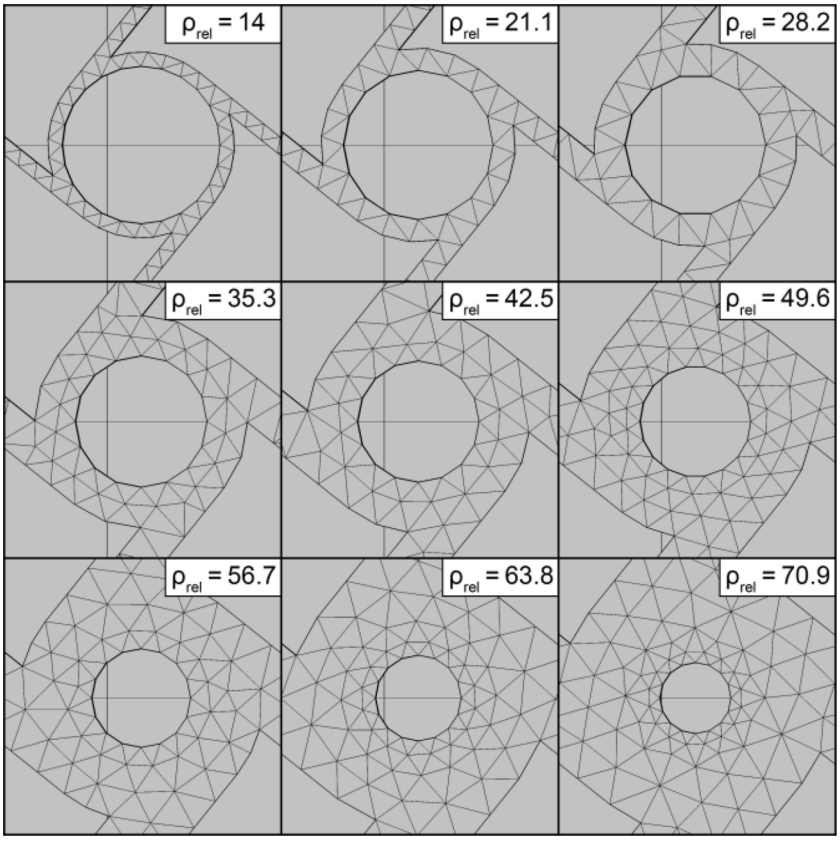


**Fig. 4.** The finite element mesh of unit cells of tetrachiral structures.

distributed force $F_y$ applied at $x = l_1$.

Within the first set of numerical experiments, the thickness of the composite plate's layers remains unchanged with the variations in the volume of solid body of the honeycombs. At the second set of experiments, the thickness of the face layers of the composite plates and the volume of solid body of the honeycombs are constant while the thickness of the honeycomb core varies within some range. It is obvious that the area of solid body of the honeycombs (Fig. 1) determines the relative density of the honeycomb core layer. In the second set of experiments, due to the constant volume of honeycombs solid body, the thickness of the honeycomb structures directly depends on the in-plane area of solid body of the honeycombs.

According to the accepted assumptions in literature (see, for example in [31–33]), for thin plates the ratio of its thickness $t$ to the smallest in-plane dimension $t/h$ (Fig. 2) should be less than 1 /5, what corresponds to composite plates in the first set of numerical experiments. However, in the second set of experiments, at small and large values of $\rho_{rel}$ the $t/h$ ratio is typical for a relatively thick and thin plate, respectively. For comparative analysis, solid plates were constructed with an equal step of increasing the volume by changing the thickness.

Strength calculations of composite plates were carried out within the framework of the theory of elasticity using the finite element method in the «COMSOL Multiphysics 5.6» numerical simulation system. Calculations were performed adopting the «Structural Mechanics» module [34]. A linear elastic body model was used to describe the behavior of the material. Under the conditions of static bending of composite and solid plates, the following boundary conditions

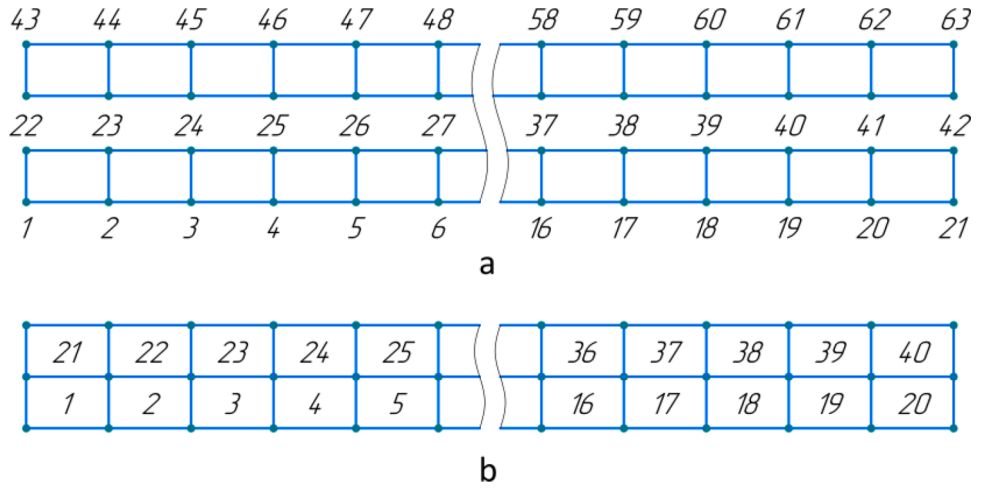


**Fig. 5.** The scheme of finite elements of a plate within the *xy*-plane: (a) global numbering of nodes, and (b) numbering of finite elements.

$$\begin{aligned} &u_{x,y,z}(0 \le x \le x_1, y = 0, 0 \le z \le h) = 0 \\ &u_{x,y,z}(x_2 \le x \le a, y = 0, 0 \le z \le h) = 0 \\ &u_{x,y,z}(0 \le x \le x_1, y = t, 0 \le z \le h) = 0 \\ &u_{x,y,z}(x_2 \le x \le a, y = t, 0 \le z \le h) = 0 \end{aligned} \tag{1}$$

and the loading condition

$$F_y = F_y(x = l_1, y = t, 0 \le z \le h) \tag{2}$$

were utilized.

To exclude the deflection in the *zy*-plane, the displacements of nodes in the face layers of composites and solid plates have been considered as $u_z = 0$.

The finite element mesh of the composite plates was constructed separately for each layer, namely: quadrangular prisms and triangular prisms were used for solid layers and honeycomb core layers, respectively (Fig. 3). The condition of continuity of field variables was established at the layer interfaces of composites. General principles were applied to construct the finite element mesh of the models. Tetrachiral honeycombs in the *xz*-plane were divided into the minimum required number of the most regular triangles while maintaining the geometric shape of the honeycombs (Fig. 4), and the face layers of the composite plates in the *xz*-plane were divided into an equal number of the most regular quadrangles. At the same time, in the first set of experiments, the tetrachiral honeycombs were divided along the thickness into two layers of finite elements, and in the second set of experiments, they contained from 1 to 7 layers according to the change in thickness. The face layers of composite plates and solid plates contained one layer of finite elements along the thickness, while the mesh of solid plates involved the most regular quadrangular prisms. The second-order serendipity family of finite elements were used in all models. Thus, calculations of composites should have approximately the same accuracy (systematic bias), which does not interfere their stress state analysis.

During static bending of composite and solid plates, the load values $F_y$ (N), have been determined, at which the maximum stresses according to the von Mises criterion were equal to the conventional yield stress of the material $\sigma_{max} = \sigma_{0.2}$.

In order to verify the results of calculations via the «COMSOL» system, additional calculations of solid plates were performed using the algorithm for solving the plane problem by the finite element method in displacements [35–37]. In the plane problem, the loading condition (2), as well as the following boundary conditions were adopted:

$$\begin{aligned} &u_{x,y,z}(x = x_1, 0 \le y \le t, 0 \le z \le h) = 0 \\ &u_{x,y,z}(x = x_2, 0 \le y \le t, 0 \le z \le h) = 0 \end{aligned} \tag{3}$$

The computational domain was divided into rectangular finite elements with four nodes at the vertices. The analytical form of the finite element stiffness matrix $k^e$ was determined by integration over the volume

$$k^e_{r,s} = \int_{\tau^e} \beta_r^T \chi \beta_s d\tau = \frac{a_{fe} b_{fe} h}{4} \int_{-1}^{1} \int_{-1}^{1} \beta_r^T \chi \beta_s d\xi d\eta \tag{4}$$

where $\beta_r$ (and also $\beta_s$) is the matrix of the relationship between nodal displacements and deformations

$$\beta_r = L\alpha_r = \begin{pmatrix} \partial/\partial x & 0 \\ 0 & \partial/\partial y \\ \partial/\partial y & \partial/\partial x \end{pmatrix} \begin{pmatrix} \psi_r & 0 \\ 0 & \psi_r \end{pmatrix} = \frac{1}{2} \begin{pmatrix} b_r & 0 \\ 0 & a_r \\ a_r & b_r \end{pmatrix} \tag{5}$$

$L$ is the matrix differential operator, $\chi$ is the matrix of elastic constants for plane deformation

$$\chi = \frac{E}{(1+\mu)(1-2\mu)} \begin{pmatrix} 1-\mu & \mu & 0 \\ \mu & 1-\mu & 0 \\ 0 & 0 & \dfrac{1-2\mu}{2} \end{pmatrix} \tag{6}$$

$a_{fe}$ and $b_{fe}$ are dimensions of the sides of the rectangular finite element along the *x*- and *y*-axes, respectively, $h$ is the size of the finite element along the *z*-axis which is equal to the width of the plate, $r$ and $s$ are numbers of matrix blocks ($r = 1, 2\ldots4$, $s = 1, 2\ldots4$), $\xi$ and $\eta$ are dimensionless coordinates of the rectangular element, $\xi_1 = -1$, $\eta_1 = -1$, $\xi_2 = 1$, $\eta_2 = -1$, $\xi_3 = 1$, $\eta_3 = 1$, $\xi_4 = -1$, $\eta_4 = 1$, $\alpha_r$ is the matrix of approximating functions, $\psi_r = (1 + \xi_r\xi)(1 + \eta_r\eta)/4$, $a_r = \eta_r(1 + \xi_r\xi)/b_{fe}$, $b_r = \xi_r(1 + \eta_r\eta)/a_{fe}$, $E$ is the longitudinal elastic modulus, and $\mu$ is the Poisson's ratio.

It was convenient to split the stiffness matrix (4) into two terms

$$k^e_{r,s} = k^E_{r,s} + k^G_{r,s} \tag{7}$$

where $k^E$ is the submatrix of normal deformations

$$k^E_{r,s} = \frac{a_{fe} b_{fe} h}{4} \int_{-1}^{1} \int_{-1}^{1} \beta_r^T \chi_E \beta_s d\xi d\eta \tag{8}$$

$k^G$ is the submatrix of shear deformations

$$k^G_{r,s} = \frac{a_{fe} b_{fe} h}{4} \int_{-1}^{1} \int_{-1}^{1} \beta_r^T \chi_G \beta_s d\xi d\eta \tag{9}$$

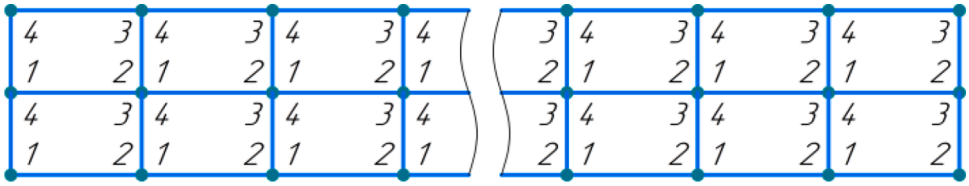


**Fig. 6.** The scheme of local numbering of nodes of finite elements.

$\chi_E$ and $\chi_G$ are the matrices of elastic constants, which have, respectively, the form

$$\chi_E = \frac{E}{(1+\mu)(1-2\mu)}\begin{pmatrix} 1-\mu & \mu & 0 \\ \mu & 1-\mu & 0 \\ 0 & 0 & 0 \end{pmatrix} \tag{10}$$

$$\chi_G = G\begin{pmatrix} 0 & 0 & 0 \\ 0 & 0 & 0 \\ 0 & 0 & 1 \end{pmatrix} \tag{11}$$

and $G$ is the shear modulus.

Calculating the integrals in (8) and (9), respectively, yields

$$k^E_{r,s} = \frac{Eh}{4(1+\mu)(1-2\mu)} \times \begin{bmatrix} (1-\mu)\gamma\xi_r\xi_s\left(1+\frac{\eta_r\eta_s}{3}\right) & \mu\xi_r\eta_s \\ \mu\eta_r\xi_s & (1-\mu)\frac{\eta_r\eta_s}{\gamma}\left(1+\frac{\xi_r\xi_s}{3}\right) \end{bmatrix} \tag{12}$$

$$k^G_{r,s} = \frac{Gh}{4}\begin{bmatrix} \frac{\eta_r\eta_s}{\gamma}\left(1+\frac{\xi_r\xi_s}{3}\right) & \eta_r\xi_s \\ \xi_r\eta_s & \gamma\xi_r\xi_s\left(1+\frac{\eta_r\eta_s}{3}\right) \end{bmatrix} \tag{13}$$

the sum of which determines the analytical expression for the stiffness matrix of the compatible finite element, where $\gamma = b_{fe}/a_{fe}$ is the dimensionless parameter.

The matrix $A$ matching the global numbers of nodes to the local numbers was constructed according to the rule $A_{m,i} = q$ with $m \in 1, 2\ldots m_f$, $i \in 1, 2\ldots i_f$, and $q \in 1, 2\ldots 4$, where $m$ is the global node number (Fig. 5,a), $m_f$ is the quantity of global nodes, $i$ is the finite element number (Fig. 5,b), $i_f$ is the quantity of finite elements, and $q$ is the local number of the node of the $i$-th finite element (Fig. 6), in so doing if $A_{m,i} \neq q$, then $A_{m,i} = 0$.

The extended stiffness matrix $k^{exp}$ was constructed according to the $k^{exp}_{m,n}(i) = k^e_{r,s}$ principle, where $r = A_{m,i}$, $s = A_{n,i}$, $m, n \in 1, 2\ldots m_f$, if $r \vee s = 0$ then $k^e_{r,s} = \begin{pmatrix} 0 & 0 \\ 0 & 0 \end{pmatrix}$

The stiffness matrix of the finite element model $K$ was determined by summing the extended stiffness matrices $K = \sum_i k^{exp}(i)$. To consider the external fixation of the finite element model node, the rows $i_1 = 2m_p - 1$, $i_2 = 2m_p$ and columns $j_1 = 2m_p - 1$, $j_2 = 2m_p$ of the stiffness matrix $K$ were deleted, where $m_p$ is the number of the fixed node.

The displacements of nodes were determined by the expression

$$u_a = K_a^{-1}P_a \tag{14}$$

where $K_a^{-1}$ is the inverse stiffness matrix with due account for the fixed nodes, $P_a = \{ P^x_{a_1} \quad P^y_{a_2} \quad \cdots \quad P^x_{a_{c-1}} \quad P^y_{a_c} \}$ is the vector of nodal forces (hereinafter, the row matrix in curly braces means the column matrix), $c = 2(m_f - p)$, $P^x_{a_{c-1}}$ and $P^y_{a_c}$ are nodal forces along $x$- and $y$-axes, respectively, and $p$ is the quantity of the fixed nodes.

The full vector of displacements $u = \{ u^x_1 \quad u^y_2 \quad \cdots \quad u^x_{e-1} \quad u^y_e \}$ ($e = 2m_f$) includes zero displacements $u_{k_o} = 0$, $o \in 1, 2$, where $k_1 = 2m_p - 1$, $k_2 = 2m_p$, and the matrix $u_a = \{ u^x_{a_1} \quad u^y_{a_2} \quad \cdots \quad u^x_{a_{c-1}} \quad u^y_{a_c} \}$ is a submatrix of $u$, where $u_{a_c} \neq 0$.

The vectors of displacements along the $x$- and $y$-axes were determined by the expressions $u^x_m = u_{m_x}$ and $u^y_m = u_{m_y}$ respectively, where $m_x = 2m - 1$, $m_y = 2m$.

The displacement vector $v$ of the nodes of the $i$-th finite element was constructed as $v_i = \{ u^x_{m^1} \quad u^y_{m^1} \quad u^x_{m^2} \quad u^y_{m^2} \quad u^x_{m^3} \quad u^y_{m^3} \quad u^x_{m^4} \quad u^y_{m^4} \}$, where $A_{m^1,i} = 1, A_{m^2,i} = 2, A_{m^3,i} = 3, A_{m^4,i} = 4$, $u^x_{m^q}$ and $u^y_{m^q}$ are the nodal displacements along the $x$- and $y$-axes, respectively.

The strain vector $\varepsilon$ of the $i$-th finite element was determined from the expression

$$\varepsilon(i,\xi,\eta) = \beta(\xi,\eta)\cdot v_i \tag{15}$$

where $\beta(\xi, \eta)$ is the matrix of the relationship between nodal displacements and deformations

$$\beta(\xi,\eta) = \frac{1}{2}\begin{pmatrix} b_a(1,\eta) & 0 \\ 0 & a_a(1,\xi) \\ b_a(2,\eta) & 0 \\ 0 & a_a(2,\xi) \\ b_a(3,\eta) & 0 \\ 0 & a_a(3,\xi) \\ b_a(4,\eta) & 0 \\ 0 & a_a(4,\xi) \end{pmatrix}^T \tag{16}$$

with $a_a(q,\xi) = \eta_q(1+\xi_q\xi)/b_{fe}$, $b_a(q,\eta) = \xi_q(1+\eta_q\eta)/a_{fe}$, and $q = 1, 2\ldots 4$.

The vector of nodal stresses $\sigma$ of the $i$-th finite element was determined as

$$\sigma(i,\xi,\eta) = \chi\varepsilon(i,\xi,\eta) \tag{17}$$

where $\xi = \xi_q$, $\eta = \eta_q$,and $\chi$ is the matrix of elastic constants obtained by excluding shear deformations from matrix (6)

$$\chi = \frac{E}{(1+\mu)(1-2\mu)}\begin{pmatrix} 1-\mu & \mu \\ \mu & 1-\mu \end{pmatrix} \tag{18}$$

The equivalent stresses $\sigma_e$ at nodes of the finite element were determined by the von Mises criterion [38]

$$\sigma_e = \sqrt{\sigma_1^2 + \sigma_2^2 - \sigma_1\sigma_2} \tag{19}$$

where $\sigma_1$ and $\sigma_2$ are the principal stresses.

For the purpose of verification, we utilized an algorithm, the expressions for which were obtained using the matrix of approximating functions described in [35]

$$\alpha^{inc}_r = \begin{pmatrix} \frac{(1+\xi_r\xi)(1+\eta_r\eta)}{4} & -\frac{\xi_r\eta_r}{8}\left(\frac{\mu}{\gamma}\xi^2 + \gamma\eta^2 - \frac{\mu}{\gamma} - \gamma\right) \\ -\frac{\xi_r\eta_r}{8}\left(\frac{1}{\gamma}\xi^2 + \mu\gamma\eta^2 - \frac{1}{\gamma} - \mu\gamma\right) & \frac{(1+\xi_r\xi)(1+\eta_r\eta)}{4} \end{pmatrix} \tag{20}$$

Repeating the previous calculations, we obtain analytical

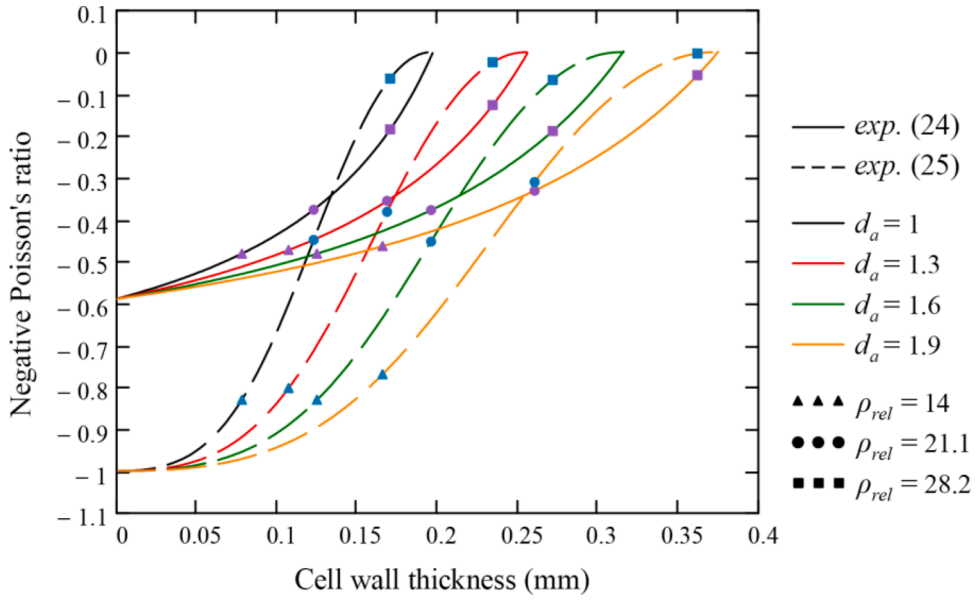


**Fig. 7.** Diagram of the cell wall thickness dependence of the NPR at different honeycombs discretization.

expressions for the submatrices $k^E_{r,s}$ and $k^G_{r,s}$ of the stiffness matrix of an incompatible finite element

$$k^E_{r,s} = \frac{Eh}{4(1+\mu)(1-2\mu)}$$

$$\times \begin{bmatrix} (1-\mu)\gamma\xi_r\xi_s\left(1+\frac{1-\mu^2}{3}\eta_r\eta_s\right) & \mu\xi_r\eta_s \\ \mu\eta_r\xi_s & (1-\mu)\frac{\eta_r\eta_s}{\gamma}\left(1+\frac{1-\mu^2}{3}\xi_r\xi_s\right) \end{bmatrix} \quad (21)$$

$$k^G_{r,s} = \frac{Gh}{4}\begin{bmatrix} \frac{\eta_r\eta_s}{\gamma} & \eta_r\xi_s \\ \xi_r\eta_s & \gamma\xi_r\xi_s \end{bmatrix} \quad (22)$$

as well as the expression for the matrix β(ξ, η) of the relationship between nodal displacements and deformations

$$\beta(\xi,\eta) = \frac{1}{2}\begin{pmatrix} b_a(1,\eta) & e_a(1,\eta) \\ c_a(1,\xi) & a_a(1,\xi) \\ b_a(2,\eta) & e_a(2,\eta) \\ c_a(2,\xi) & a_a(2,\xi) \\ b_a(3,\eta) & e_a(3,\eta) \\ c_a(3,\xi) & a_a(3,\xi) \\ b_a(4,\eta) & e_a(4,\eta) \\ c_a(4,\xi) & a_a(4,\xi) \end{pmatrix}^T \quad (23)$$

where $c_a(q,\xi) = -\mu\xi_q\eta_q\xi/b_{fe}$, and $e_a(q,\eta) = -\mu\xi_q\eta_q\eta/a_{fe}$.

When calculating solid plates using the above algorithms for solving the plane problem, the plates were divided along the thickness into two layers of rectangular finite elements with approximately equal sides.

## 3. Numerical results and discussion

Let us construct a diagram of the cell wall thickness of the investigated tetrachiral honeycombs dependence of the negative Poisson's ratio (NPR) (Fig. 7) using the following analytical expressions proposed in [19] and [21], respectively:

$$\mu = -\frac{\sin\theta[\alpha_h - \alpha_h(\pi - 2\theta)(\alpha_h + \beta_h)]}{2\alpha_h(\alpha_h - \alpha_h\sin\theta - \beta_h\sin\theta)} \quad (24)$$

where $\alpha_h = \frac{r_a}{l}, \beta_h = \frac{t_{sw}}{l}$, and

$$\mu = -\frac{(a_h - b_h)^2\sin^2\theta\cos^2\theta}{2a_hb_h(sin^4\theta + \cos^4\theta) + (a_h + b_h)^2\sin^2\theta\cos^2\theta} \quad (25)$$

where $a_h = \frac{l_e^3}{24EI}$, $b_h = \frac{l}{2t_ht_{sw}E}$, $l_e = l - 2\sqrt{2rt_{sw} - t_{sw}^2}$, $I = \frac{t_ht_{sw}^3}{12}$, and $t_h$ is the honeycomb thickness.

The considered honeycombs at small values of relative density (14, 21.1, and 28.2) possess NPR. At the same time, for structures with different discretization, but equal $\rho_{rel}$, the NPR values lie within a narrow range. With an increase in $\rho_{rel}$, Poisson's ratio goes from negative values to positive ones.

For calculations the following parameter values were taken for composite and solid plates (Fig. 2): $a = 54$ mm, $h = 13$ mm, $l_1 = a/2$, $x_1 = 12$ mm, and $x_2 = 42$ mm. For the first set of numerical experiments, the thickness of the honeycomb core layers is 1 mm. For the second set of experiments, the volume of solid body of the honeycomb structures is 351 mm$^3$. In both formulations, the thickness of the face layers is 0.5 mm.

The properties of the Formlabs Clear photopolymer resin [39] were used as the material properties of composite and solid plates, namely: $E = 2.8$ GPa, $\mu = 0.35$, density $\rho = 1200$ kg/m$^3$, and conventional yield strength $\sigma_{0.2} = 35$ MPa, which was determined in accordance with the graph provided by Formlabs [40]. Assume that the Formlabs Clear material is isotropic with a slight difference in tensile and compressive strength.

The composite plates under investigation have the welded contact at the interface between the layers, what made it possible to consider them as a monolithic polymer structure with the possibility of layer-by-layer stress analysis. It has been noted in [41,42] that the utilization of the von Mises criterion when calculating the limiting state of polymers results in a good agreement with experimental data. Due to the ease of use and satisfactory results, this criterion is widely applied in the analysis of the stress state of polymer structures [43–47].

The verification of the «COMSOL» system by the example of calculations of solid plates has allowed us to demonstrate a good matching of the results obtained using the «Structural Mechanics» module and two above-mentioned algorithms for solving the plane problem by

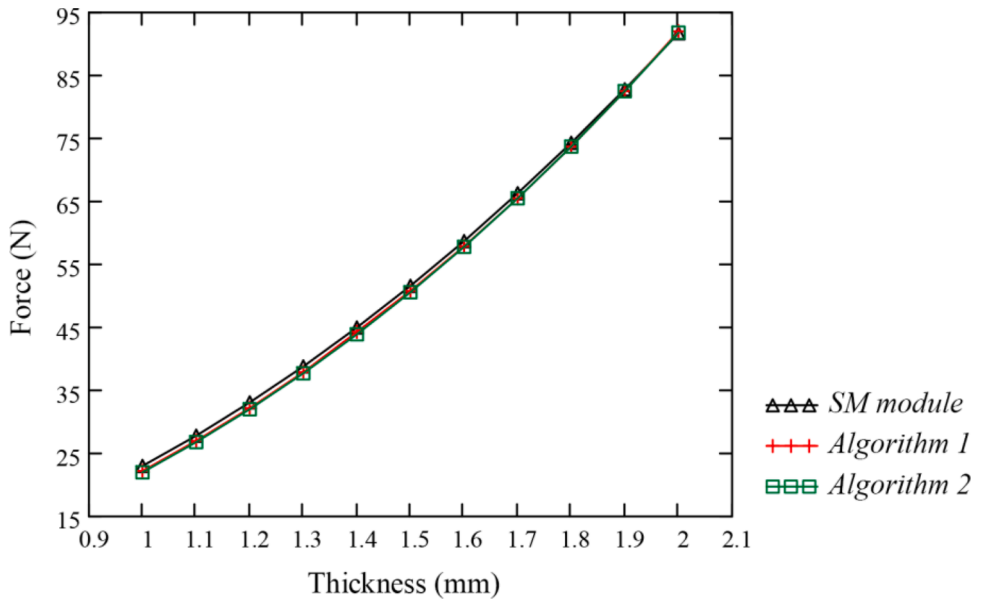


**Fig. 8.** Diagram of the solid plate's thickness dependence of the load $F_y$ at $\sigma_{max} = \sigma_{0.2}$.

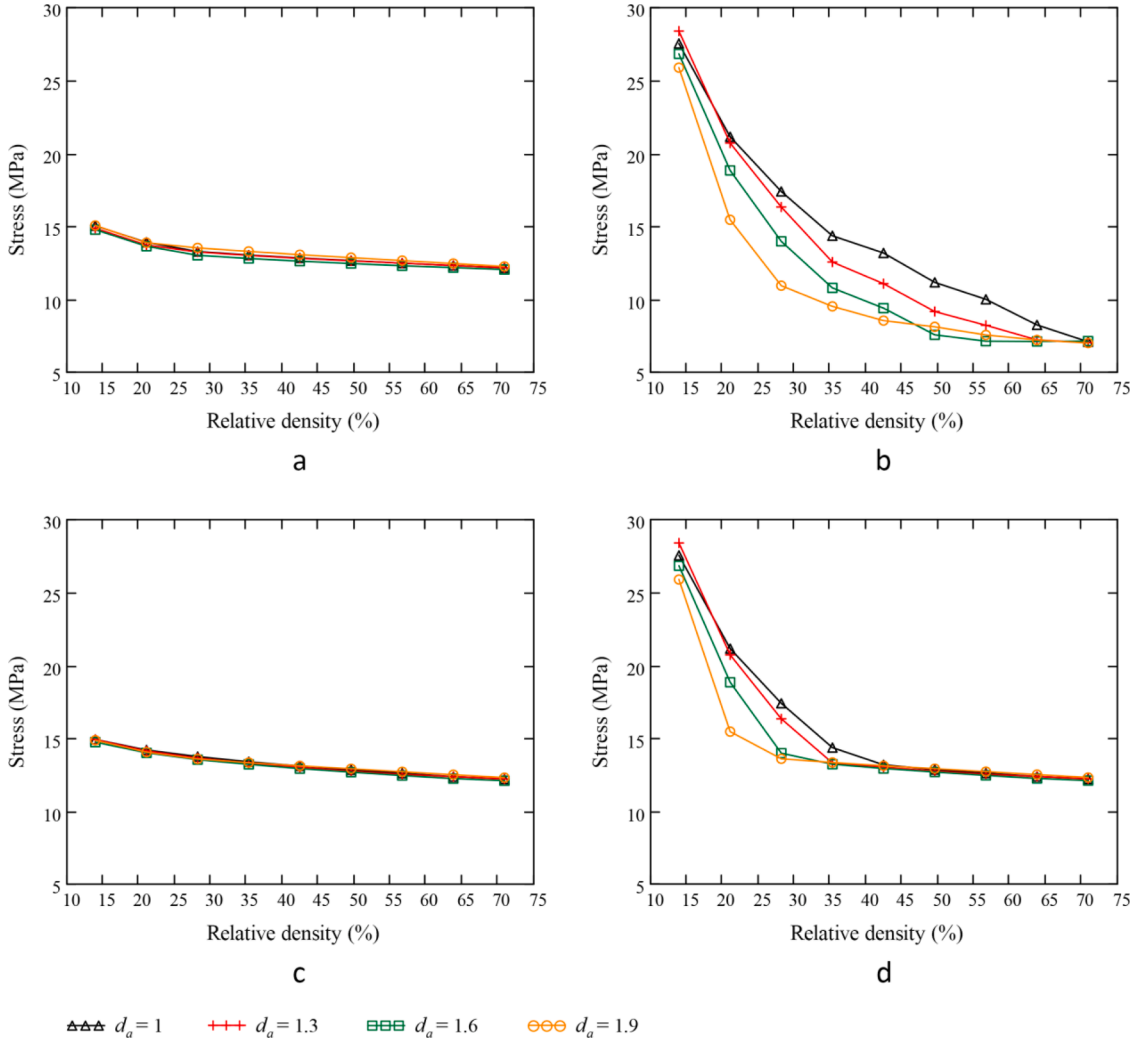


**Fig. 9.** Diagrams of the honeycomb cores relative density dependence of the maximum stresses at $F_y = 30$ N in the first formulation of numerical experiments: a) in the upper solid layer, b) in the honeycomb core layer, c) in the lower solid layer, d) in the thin composite plate.

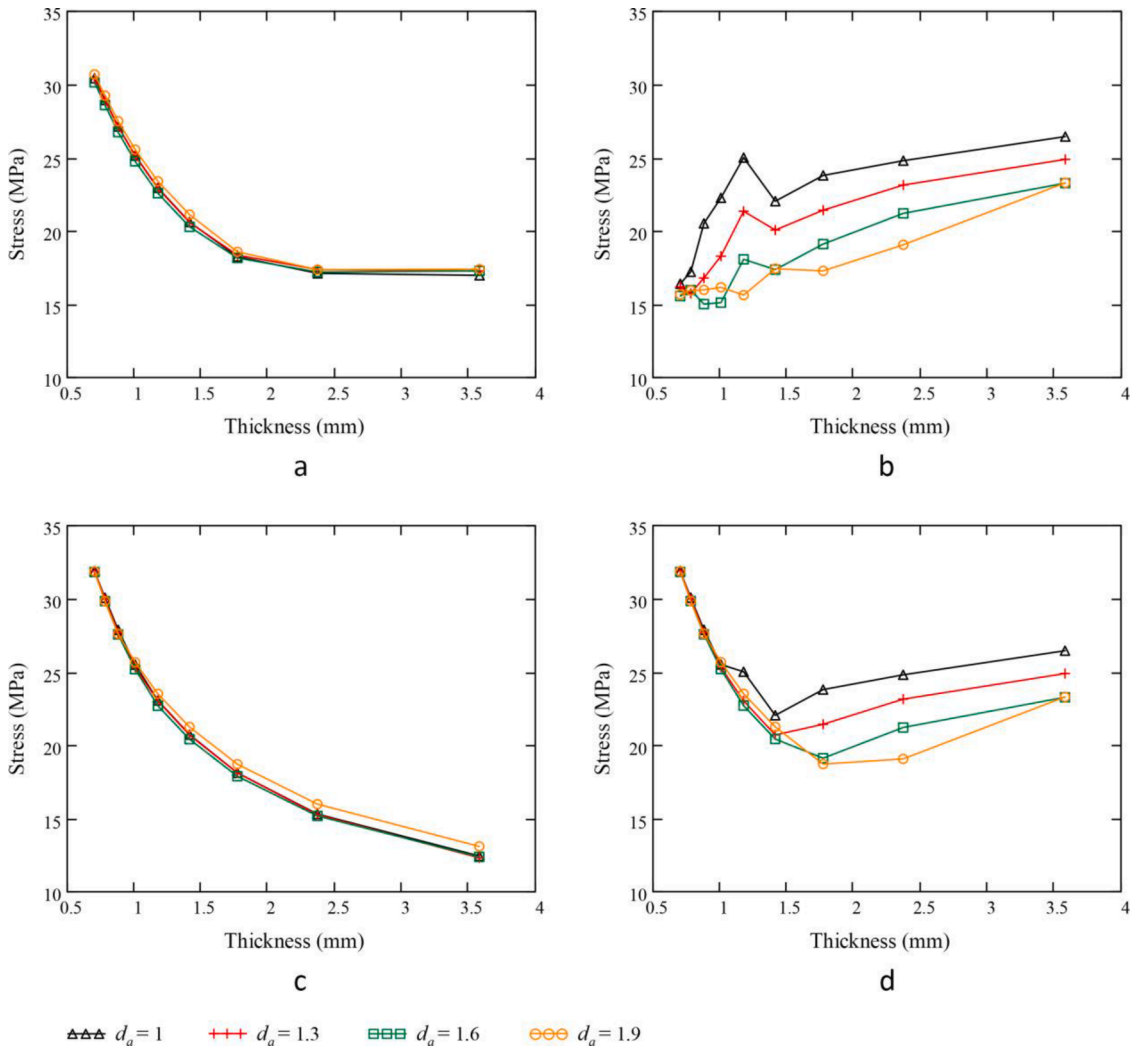


**Fig. 10.** Diagrams of the honeycombs thickness dependence of the maximum stresses at $F_y = 60$ N in the second formulation of numerical experiments: a) in the upper solid layer, b) in the honeycomb core layer, c) in the lower solid layer, d) in the composite plate.

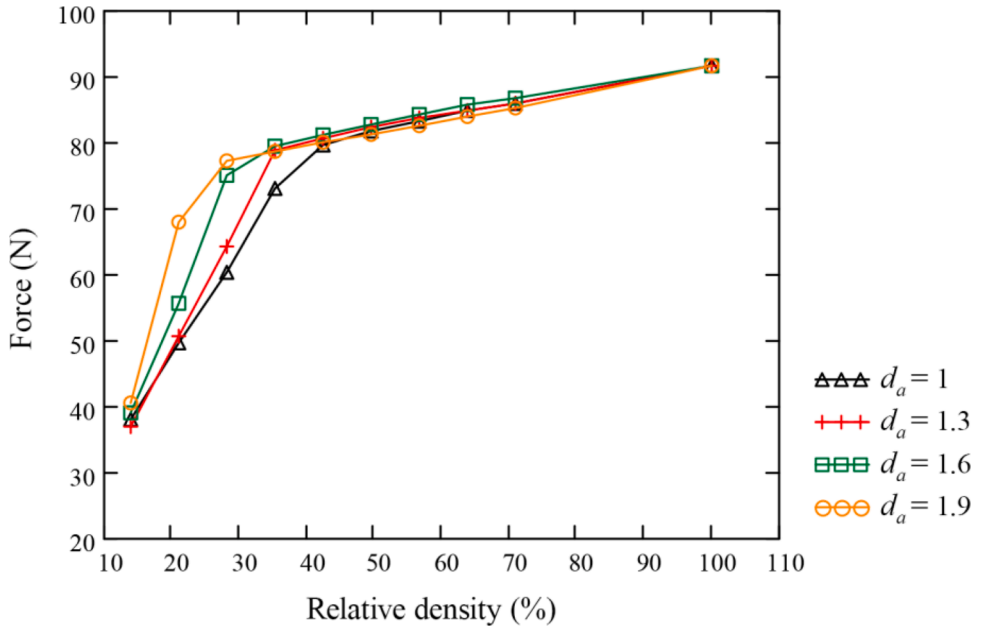


**Fig. 11.** Diagram of the honeycomb cores relative density dependence of the load $F_y$ at $\sigma_{max} = \sigma_{0.2}$ for the first set of numerical experiments.

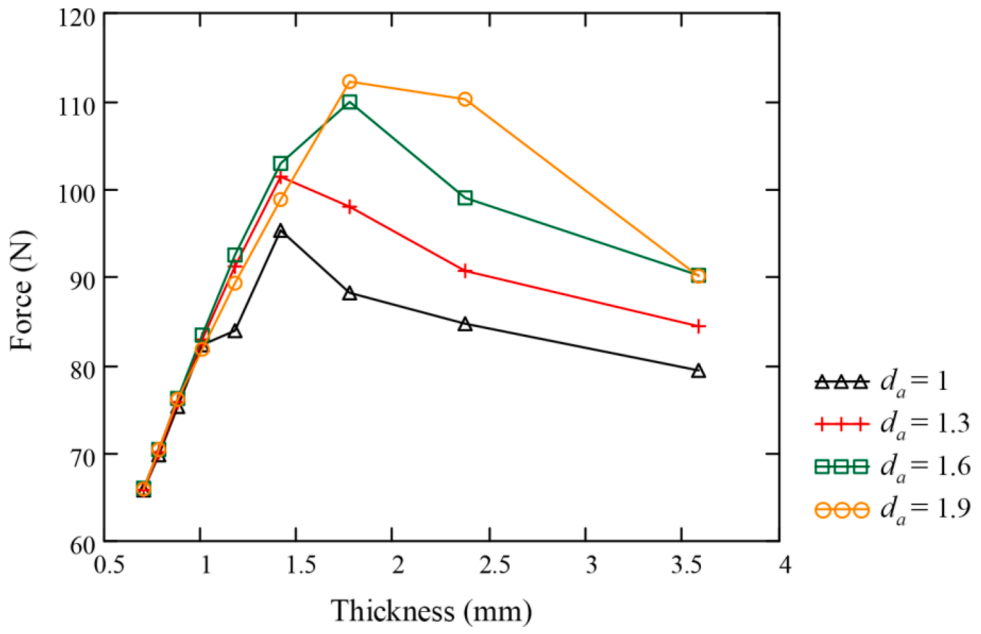


**Fig. 12.** Diagram of the honeycombs thickness dependence of the load $F_y$ at $\sigma_{max} = \sigma_{0.2}$ for the second set of numerical experiments.

comparing the graphs constructed in Fig. 8.

Fig. 9 shows the diagrams of the honeycomb cores relative density dependence of the maximum stresses in the layers of thin composite plates at $F_y = 30$ N in the first set of numerical experiments. Within the variation of $\rho_{rel}$ from 14 to 71%, the difference between the values of the maximum stresses in tetrachiral honeycombs with different discretization has a pronounced area of the increase and subsequent decrease.

In so doing, the discretization of honeycomb structures does not affect the values of the maximum stresses in the solid layers of the composite plates, while the values of the stresses in the upper and lower solid layers are almost equal. The diagram in Fig. 9,d displays the highest stresses when three layers were taken into account simultaneously, i.e. directly in the composite plate. At small values of $\rho_{rel}$, the maximum stresses in the composite plates appear first in the tetrachiral honeycombs, and with the increase in $\rho_{rel}$ they transfer to solid layers. The honeycomb structures with lower discretization demonstrate the higher strength relative to the structures with the higher discretization. The transition of critical stresses within composite plates from honeycomb core layers to solid layers occurs in honeycombs with less discretization at a lower relative density.

Fig. 10 shows the diagrams of the honeycombs thickness dependence of the maximum stresses in the layers of composite plates at $F_y = 60$ N in the second set of numerical experiments. The relative density of tetrachiral honeycombs varies in the same range as in the first set of experiments. However, due to the equal volume of the solid body, the honeycombs have different thicknesses, which increase with decreasing $\rho_{rel}$. The maximum stresses in tetrachiral honeycombs with different discretization increase nonmonotonically with an increase in the

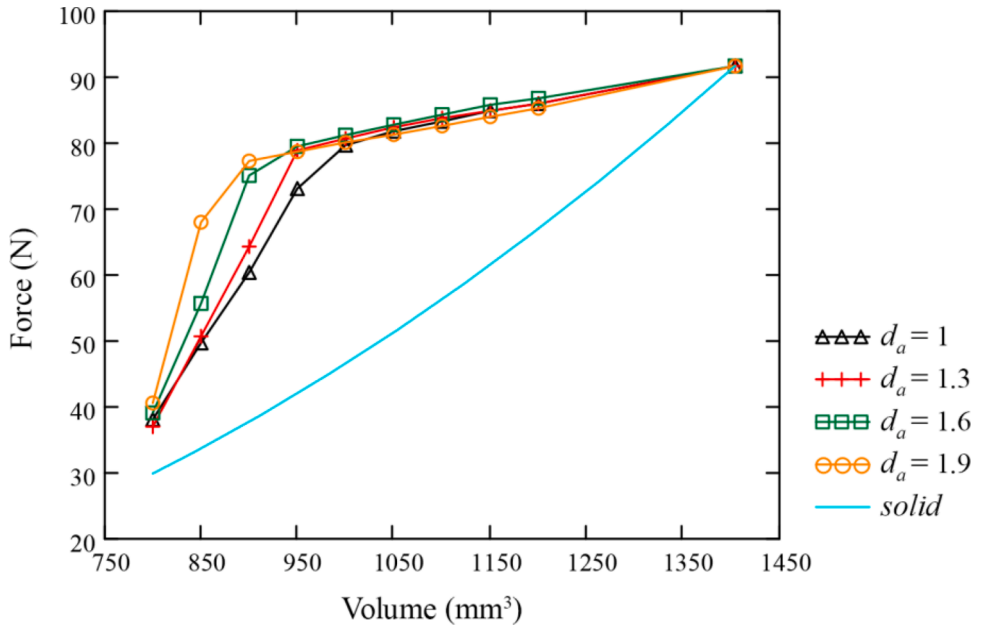


**Fig. 13.** Diagram of the volume of solid body of the composite and solid plates dependence of the load $F_y$ at $\sigma_{max} = \sigma_{0.2}$ for the first formulation of numerical experiments.

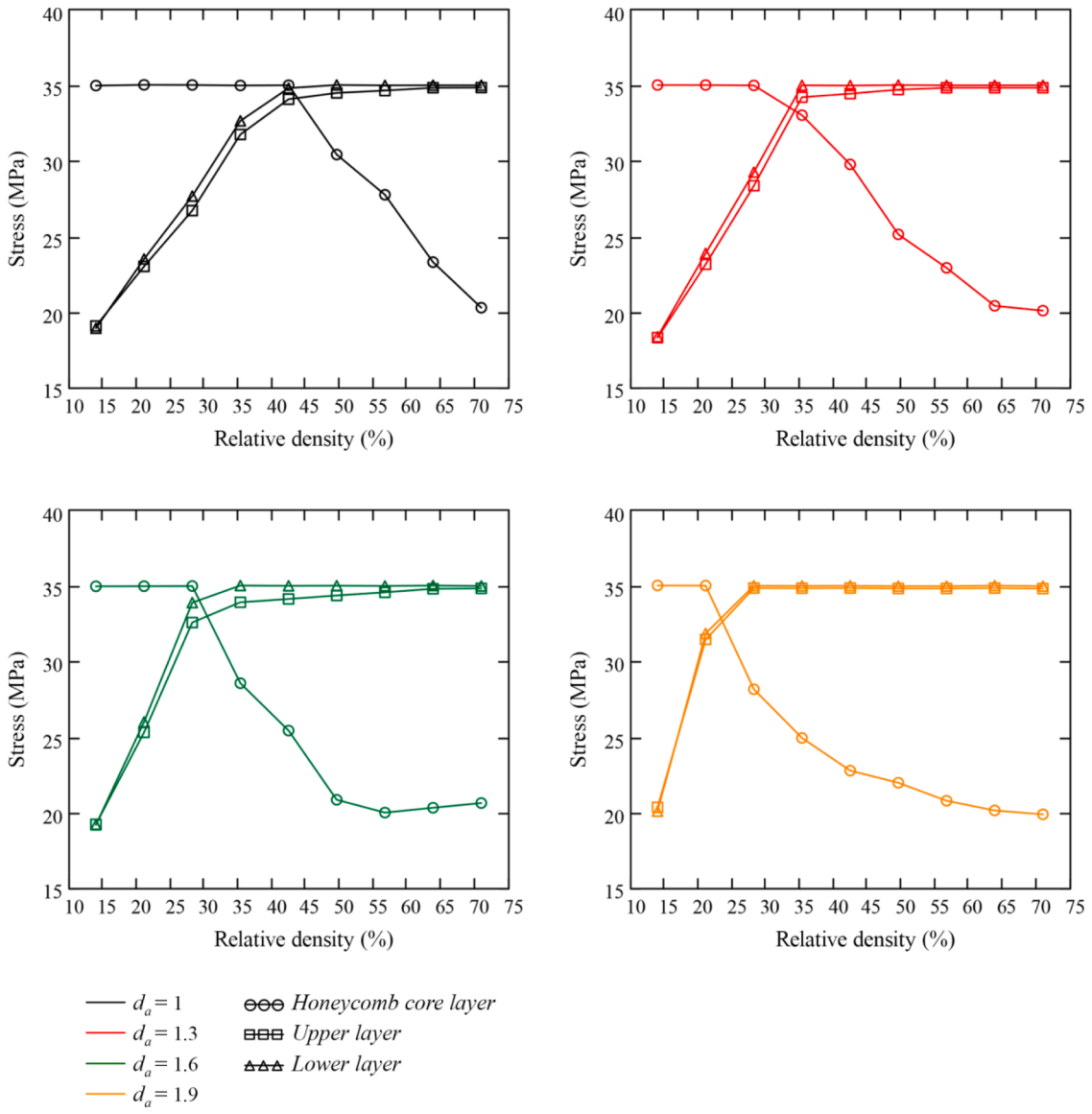


**Fig. 14.** Diagrams of the honeycomb cores relative density dependence of the maximum stresses in the layers of thin composite plates for the first formulation of numerical experiments.

honeycombs thickness (decrease in $\rho_{rel}$), but the intensity of this increase is lower relative to data presented in Fig. 9,b. The values of the maximum stresses in solid layers of composite plates do not depend on the discretization of honeycomb structures. At small values of the honeycombs thickness, the stresses in the upper and lower solid layers have an insignificant difference, which increases with the increase in the thickness. In the second set of experiments, the honeycombs with lower discretization also show higher strength relative to structures with higher discretization. The sequence of transition of critical stresses from honeycomb core layers to solid layers occurs in a similar way as in the first set of experiments.

In addition, diagrams of the honeycomb cores relative density (Fig. 11) and thickness (Fig. 12) dependence of the load $F_y$ at $\sigma_{max} = \sigma_{0.2}$ are presented, respectively, for the first and second sets of numerical experiments. It is easy to notice that the form of the graphs in Fig. 11 and Fig. 12 is the symmetrical reflection of the graphs in Fig. 9,d and Fig. 10, d, respectively. From the diagram in Fig. 12 it follows that with a constant volume of honeycombs solid body, the variation in their thickness by changing the relative density allows one to obtain the maximum strength of the composite plates. At the same time, the peak strength value is at the point of transition of maximum stresses from honeycomb core layers to solid layers at a certain honeycombs thickness.

The diagram of the volume of solid body of the thin composite and solid plates dependence of the load $F_y$ at $\sigma_{max} = \sigma_{0.2}$ for the first set of numerical experiments is constructed in Fig. 13. The diagram shows that with an increase in the volume of solid body of the honeycomb core layer until reaching a continuous medium, the strength of composites tends to the strength of a solid plate with the same external dimensions. At the same time, with an increase in the volume of solid body of the honeycombs, the change in critical stresses in composites becomes linear (Fig. 13), until a complete transition from honeycombs to a continuous medium. This observation may indicate a satisfactory accuracy of numerical experiments of composite plates, provided the corresponding accuracy of calculations for solid plates. The diagram also shows that thin composite plates could significantly reduce the volume of a solid body relative to solid plates with equal strength and insignificant difference along the thickness.

The diagram of the honeycomb core relative density dependence of the maximum stresses in the layers of composite plates at $\sigma_{max} = \sigma_{0.2}$ in the first and second sets of numerical experiments are presented, respectively, in Fig. 14 and Fig. 15. With the increase in $\rho_{rel}$ at both types of experiments, the transition of critical stresses in composites with a

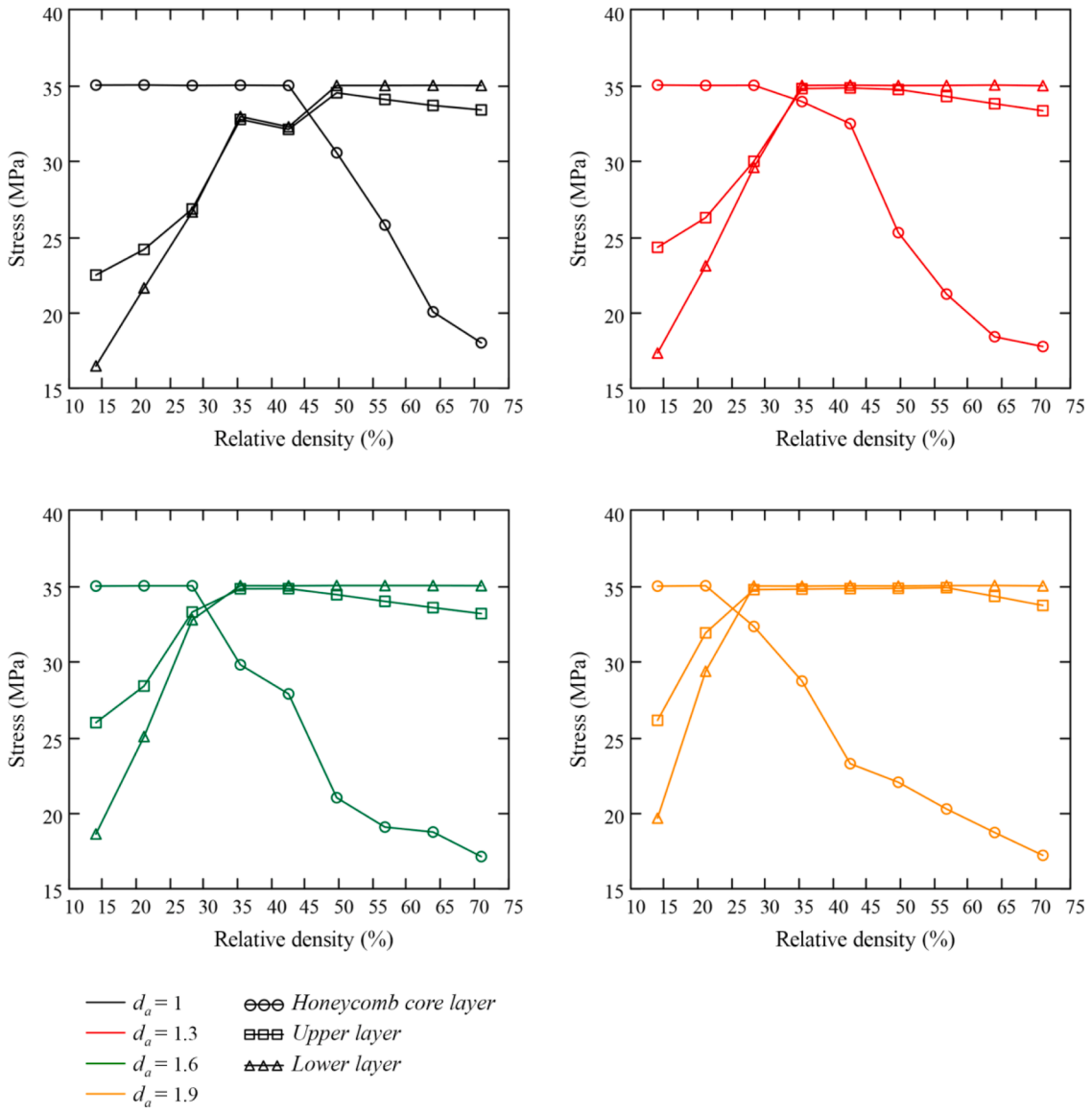


**Fig. 15.** Diagrams of the honeycomb cores relative density dependence of the maximum stresses in the layers of composite plates for the second formulation of numerical experiments.

honeycomb core layer to solid layers occurs with the same sequence within equal ranges.

Fig. 16 shows the diagrams of stress distribution in composite plates at $d_a \in 1.6$, $\rho_{rel} = 14$, $\sigma_{max} = \sigma_{0.2}$ in two formulations of numerical experiments. Critical stresses in relatively thick composite plates are localized mainly in the area of application of the force, and in thin composite plates they have a more uniform distribution.

## Conclusions

In this work, the influence of discretization, relative density and thickness of a honeycomb core on the stress state of three-layered composite plates with a tetrachiral honeycomb interlayer during static bending with rigidly clamped ends was investigated. In the first set of numerical experiments, the volume of honeycombs solid body was varied under a constant thickness of layers, and in the second set of experiments, the thickness of the honeycomb structures was varied at a constant volume of honeycombs solid body and the thickness of the face layers. It has been found that in the first formulation under conditions of constant loading on composites, with an increase in the relative density of honeycombs from 14 to 71%, the difference between the maximum stresses in honeycombs with different discretization has a pronounced area of increase and subsequent decrease. It has been shown that thin composite plates possessed the significantly reduced volume of a solid body relative to solid plates with equal strength and insignificant difference in thickness. In the second type of experiments under constant load conditions, the maximum stresses in the tetrachiral honeycombs increase nonmonotonically with the increase in the thickness of honeycombs (or with the decrease in the relative density), but the intensity of the increase is lower relative to the first formulation. With a constant volume of honeycombs solid body, variation in their thickness by changing the relative density (i.e. cell wall thickness) allows one to reach the maximum strength of composite plates. In so doing, the peak strength value is at the point of transition of maximal stresses from honeycomb core layers to solid layers at a certain thickness of honeycombs. In both sets of experiments, honeycomb structures with lower discretization show higher strength relative to structures with higher discretization. In addition, in both formulations, the discretization of honeycombs does not affect the values of the maximal stresses in solid layers of composite plates. Critical stresses in relatively thick composite plates are localized mainly in the area of force application, while in thin composite plates they have a more uniform distribution.

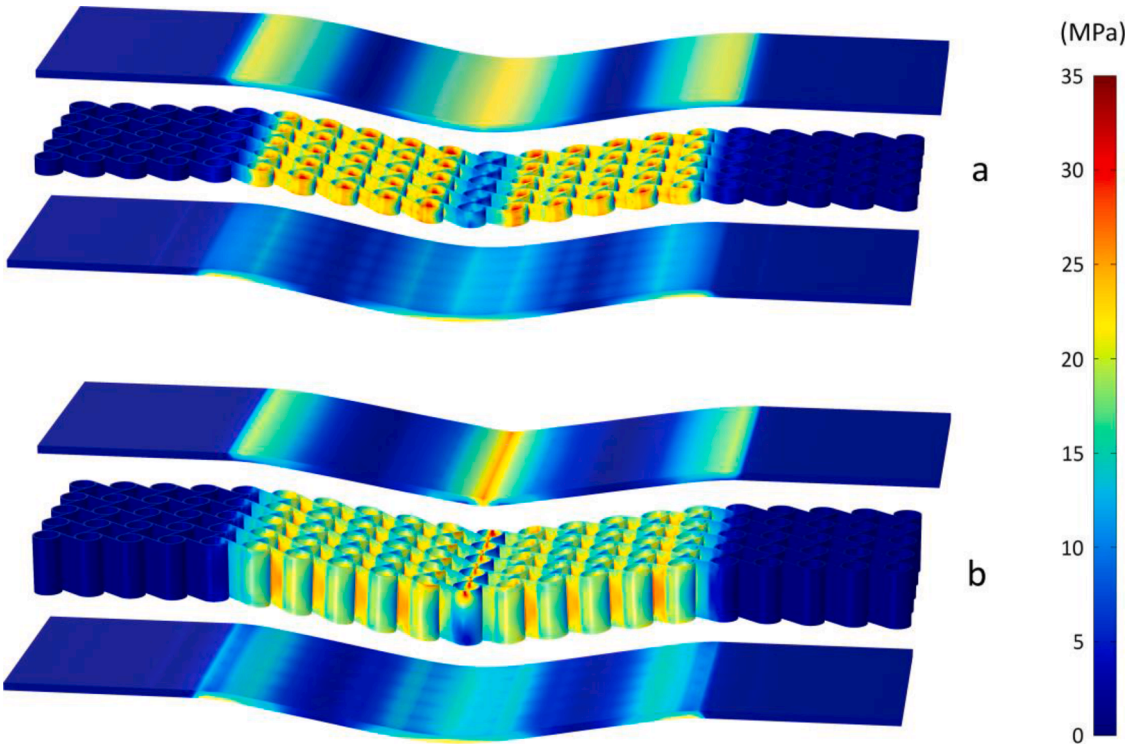


**Fig. 16.** Diagrams of the stress distribution in a thin (a) and relatively thick (b) composite plate at $\sigma_{max} = \sigma_{0.2}$.

The procedure described could be generalized for other types of static loading and boundary conditions, as well as for multi-layer plates.

## Funding

The reported study was funded by RFBR, project number 20–38–90025.

## Declaration of Competing Interest

The authors declare that they have no known competing financial interests or personal relationships that could have appeared to influence the work reported in this paper.

## Acknowledgement

The studies have been carried out using the facilities of the Collective Research Center named after Professor Yu. M. Borisov, Voronezh State Technical University, which is partly supported by the Ministry of Science and Education of the Russian Federation, Contract No 075–15–2021–662.

## References

[1] K.E. Evans, Auxetic polymers: a new range of materials, Endeavour 15 (4) (1991) 170–174, https://doi.org/10.1016/0160-9327(91)90123-S.
[2] R.V. Goldstein, V.A. Gorodtsov, D.S. Lisovenko, Auxetic mechanics of crystalline materials, Mech. Solids 45 (4) (2010) 529–545, https://doi.org/10.3103/S0025654410040047.
[3] R.S. Lakes, Negative-Poisson's-ratio materials: auxetic solids, Annu. Rev. Mater. Res. 47 (2017) 63–81, https://doi.org/10.1146/annurev-matsci-070616-124118.
[4] X. Ren, R. Das, P. Tran, T.D. Ngo, Y.M. Xie, Auxetic metamaterials and structures: a review, Smart Mater. Struct. 27 (2) (2018), 023001, https://doi.org/10.1088/1361-665X/aaa61c.
[5] P.U. Kelkar, H.S. Kim, K.H. Cho, J.Y. Kwak, C.Y. Kang, H.C. Song, Cellular auxetic structures for mechanical metamaterials: a review, Sensors 20 (11) (2020) 3132, https://doi.org/10.3390/s20113132.
[6] J. Zhang, G. Lu, Z. You, Large deformation and energy absorption of additively manufactured auxetic materials and structures: a review, Compos. B. Eng. (2020), 108340, https://doi.org/10.1016/j.compositesb.2020.108340.
[7] A. Love, A Treatise On the Mathematical Theory of Elasticity, Cambridge University Press, Cambridge, 1892. https://hal.archives-ouvertes.fr/hal-01307751.
[8] L.D. Landau, E.M. Lifshitz, Course of Theoretical Physics Vol 7: Theory and Elasticity, Pergamon press, Oxford, 1959.
[9] A.V. Mazaev, O. Ajeneza, M.V. Shitikova, Auxetics materials: classification, mechanical properties and applications, IOP Conf. Ser. Mater. Sci. Eng. 747 (1) (2020), 012008, https://doi.org/10.1088/1757-899X/747/1/012008.
[10] V. Birman, G.A. Kardomateas, Review of current trends in research and applications of sandwich structures, Compos. B. Eng. 142 (2018) 221–240, https://doi.org/10.1016/j.compositesb.2018.01.027.
[11] Y. Feng, H. Qiu, Y. Gao, H. Zheng, J. Tan, Creative design for sandwich structures: a review, Int. J. Adv. Robot. Syst. 17 (3) (2020), 1729881420921327, https://doi.org/10.1177/1729881420921327.
[12] A. Lorato, P. Innocenti, F. Scarpa, A. Alderson, K.L. Alderson, K.M. Zied, N. Ravirala, W. Miller, C.W. Smith, K.E. Evans, The transverse elastic properties of chiral honeycombs, Compos. Sci. Technol. 70 (7) (2010) 1057–1063, https://doi.org/10.1016/j.compscitech.2009.07.008.
[13] A. Alderson, K.L. Alderson, D. Attard, K.E. Evans, R. Gatt, J.N. Grima, W. Miller, N. Ravirala, C.W. Smith, K. Zied, Elastic constants of 3-, 4-and 6-connected chiral and anti-chiral honeycombs subject to uniaxial in-plane loading, Compos. Sci. Technol. 70 (7) (2010) 1042–1048, https://doi.org/10.1016/j.compscitech.2009.07.009.
[14] Y. Chen, X. Liu, G. Hu, Micropolar modeling of planar orthotropic rectangular chiral lattices, CR Mecanique 342 (5) (2014) 273–283, https://doi.org/10.1016/j.crme.2014.01.010.
[15] Y. Chen, X.N. Liu, G.K. Hu, Q.P. Sun, Q.S. Zheng, Micropolar continuum modelling of bi-dimensional tetrachiral lattices, Proc. Math. Phys. Eng. Sci. 470 (2165) (2014), 20130734, https://doi.org/10.1098/rspa.2013.0734.
[16] A. Bacigalupo, L. Gambarotta, Homogenization of periodic hexa-and tetrachiral cellular solids, Compos. Struct. 116 (2014) 461–476, https://doi.org/10.1016/j.compstruct.2014.05.033.
[17] D. Mousanezhad, B. Haghpanah, R. Ghosh, A.M. Hamouda, H. Nayeb-Hashemi, A. Vaziri, Elastic properties of chiral, anti-chiral, and hierarchical honeycombs: a simple energy-based approach, Theor. Appl. Mech. Lett. 6 (2) (2016) 81–96, https://doi.org/10.1016/j.taml.2016.02.004.
[18] R. Zhong, M. Fu, Q. Yin, O. Xu, L. Hu, Special characteristics of tetrachiral honeycombs under large deformation, Int. J. Solids Struct. 169 (2019) 166–176, https://doi.org/10.1016/j.ijsolstr.2019.04.020.
[19] C. Qi, F. Jiang, C. Yu, S. Yang, In-plane crushing response of tetra-chiral honeycombs, Int. J. Impact Eng. 130 (2019) 247–265, https://doi.org/10.1016/j.ijimpeng.2019.04.019.
[20] A. Alomarah, S.H. Masood, I. Sbarski, B. Faisal, Z. Gao, D. Ruan, Compressive properties of 3D printed auxetic structures: experimental and numerical studies, Virtual Phys. Prototyp. 15 (1) (2020) 1–21, https://doi.org/10.1080/17452759.2019.1644184.

[21] X. Lu, V.B.C. Tan, T.E. Tay, Auxeticity of monoclinic tetrachiral honeycombs, Compos. Struct. 241 (2020), 112067, https://doi.org/10.1016/j.compstruct.2020.112067.
[22] F.L. Scarpa, G.R. Tomlinson, Vibroacoustics and damping analysis of negative Poisson's ratio honeycombs, Proc. SPIE, Smart Structures and Materials: Passive Damping and Isolation 3327 (1998) 339–348.
[23] C. Lira, F. Scarpa, R. Rajasekaran, A gradient cellular core for aeroengine fan blades based on auxetic configurations, J. Intell. Mater. Syst. Struct. 22 (9) (2011) 907–917, https://doi.org/10.1177/1045389×11414226.
[24] T. Li, L. Wang, Bending behavior of sandwich composite structures with tunable 3D-printed core materials, Compos. Struct. 175 (2017) 46–57, https://doi.org/10.1016/j.compstruct.2017.05.001.
[25] D. Xiao, X. Chen, Y. Li, W. Wu, D. Fang, The structure response of sandwich beams with metallic auxetic honeycomb cores under localized impulsive loading-experiments and finite element analysis, Mater. Des. 176 (2019), 107840, https://doi.org/10.1016/j.matdes.2019.107840.
[26] K. Essassi, J.L. Rebiere, A. El Mahi, M.A. Ben Souf, A. Bouguecha, M. Haddar, Investigation of the static behavior and failure mechanisms of a 3D printed bio-based sandwich with auxetic core, Int. J. Appl. Mech. 12 (5) (2020), 2050051, https://doi.org/10.1142/S1758825120500519.
[27] J. Smardzewski, Experimental and numerical analysis of wooden sandwich panels with an auxetic core and oval cells, Mater. Des. 183 (2019), 108159, https://doi.org/10.1016/j.matdes.2019.108159.
[28] K. Peliński, J. Smardzewski, Bending behavior of lightweight wood-based sandwich beams with auxetic cellular core, Polymers (Basel) 12 (8) (2020), 1723, https://doi.org/10.3390/polym12081723.
[29] A.V. Mazaev, Strength analysis of composite plates with auxetic honeycomb at static bending by the finite element method, IOP Conf. Ser. Mater. Sci. Eng. 1129 (1) (2021), 012007, https://doi.org/10.1088/1757-899X/1129/1/012007.
[30] A.V. Mazaev, M.V. Shitikova, Static bending strength of sandwich composite plates with tetrachiral honeycombs, Int. j. comput. civ. struct. eng. 17 (3) (2021) 104–115, https://doi.org/10.22337/2587-9618-2021-17-2-104-115.
[31] N.I. Bezukhov, Fundamentals of the Theory of elasticity, Plasticity and Creep, Vysshaya Shkola, Moscow, 1968 in Russian.
[32] V.P. Suslov, Yu.P. Kochanov, V.N. Spikhtarenko, Structural Mechanics of a Ship and the Foundations of the Theory of Elasticity, Sudostroenie, Leningrad, 1972 in Russian.
[33] V.V. Chuvatov, Calculation of Plates For Strength and Stability By the Mesh Method, UPI edition, 1972 in RussianSverdlovsk.
[34] A.B. COMSOL, Structural Mechanics Module User's Guide, COMSOL AB, Stockholm, 2020.
[35] I.F. Obraztsov, L.M. Savel'ev, K.S. Khazanov, Finite Element Method in Problems of Structural Mechanics of Aircraft, Vysshaya Shkola, Moscow, 1985 in Russian.
[36] O.C. Zienkiewicz, P.B. Morice, The Finite Element Method in Engineering Science, McGraw-Hill, London, 1971.
[37] D.H. Norrie, G. de Vries, An Introduction to Finite Element Analysis, Academic Press, London, 1978.
[38] Yu.N. Rabotnov, Resistance of Materials, Fizmatgiz, Moscow, 1962 in Russian.
[39] Formlabs, Material Data Sheet: Standard, Formlabs, Somerville, 2017.
[40] Hubs, SLA 3D printing materials compared. www.hubs.com/knowledge-base/sla-3d-printing-materials-compared, 2021 (accessed 15 August 2021).
[41] H.H. Kausch, Polymer Fracture, Springer-Verlag, Berlin, 1978.
[42] A.Ya. Goldman, Strength of Structural Plastics, Mashinostroenie, Leningrad, 1979 in Russian.
[43] A. Airoldi, P. Bettini, M. Zazzarini, F. Scarpa, Failure and energy absorption of plastic and composite chiral honeycombs, WIT Trans. Built Environ. 126 (2012) 101–114, https://doi.org/10.2495/SU120091.
[44] C. Yang, H.D. Vora, Y. Chang, Behavior of auxetic structures under compression and impact forces, Smart Mater. Struct. 27 (2) (2018), 025012, https://doi.org/10.1088/1361-665X/aaa3cf.
[45] H. Araújo, M. Leite, A.R. Ribeiro, A.M. Deus, L. Reis, M.F. Vaz, The effect of geometry on the flexural properties of cellular core structures, Proc. Inst. Mech. Eng., Part L 233 (3) (2019) 338–347, https://doi.org/10.1177/1464420718805511.
[46] J. Chen, W. Chen, H. Hao, S. Huan, W. Tao, Mechanical behaviors of 3D re-entrant honeycomb polyamide structure under compression, Mater. Today Commun. 24 (2020), 101062, https://doi.org/10.1016/j.mtcomm.2020.101062.
[47] E. Provaggi, C. Capelli, B. Rahmani, G. Burriesci, D.M. Kalaskar, 3D printing assisted finite element analysis for optimising the manufacturing parameters of a lumbar fusion cage, Mater. Des. 163 (2019), 107540, https://doi.org/10.1016/j.matdes.2018.107540.